

UNSTEADY PARALLEL FLOW OF AN ELASTO-VISCO-HYPOPLASTIC FLUID BETWEEN TWO INFINITE PARALLEL PLATES

C. Fang¹ and C.H. Lee²

¹Assistant Professor, Dept. of Civil Engineering, Cheng Kung University, Chinese Taiwan

²Ph. D. student, Dept. of Hydraulic and Ocean Engineering, Cheng Kung University, Chinese Taiwan

Email: cfang@mail.ncku.edu.tw; n8895109@mail.ncku.edu.tw

ABSTRACT :

An evolution equation for the Cauchy stress tensor is proposed to take elastic, viscous and plastic characteristics of complex fluids simultaneously into account. In particular, hypoplasticity is incorporated to account for the plastic features. The stress model is applied to investigate time-dependent flows of an elasto-visco-plastic fluid between two infinite parallel plates driven by the oscillating motions of the plate to study the cyclic responses and the model performance. Numerical simulations show that while different degrees of elastic and viscous effects can be captured by varying the model parameters, plastic deformation plays a significant role in the velocity distribution, and can be simulated appropriately by use of hypoplasticity. The stress model is capable of accounting for the combined elastic, viscous and plastic features of complex materials in transient motions, and applications may be found in geomorphic fluid motions like soil liquefaction or debris flows induced by seismic activities.

KEYWORDS: stress tensor, hypoplasticity, soil liquefaction

1. INTRODUCTION

Materials are classified into different kinds according to their responses to external excitations (force, temperature difference, etc.), e.g. solids are traditionally defined as materials which can sustain shear stress, whilst fluids are those which deforms continuously under an applied shear stress [1,2]. Since the external excitation may be maintained either in a very short or a very long period of time, the material responses of a specific material can have a dramatic change regarding the duration of the external excitation. As a result, the above traditional classification is not strictly accurate and should be supplemented by considering the effects of the *Deborah number* from the macroscopic point of view, which is defined as the ratio of the material characteristic time scale divided by the characteristic time scale of the external excitation. Materials behave like solids when the Deborah number is high, whilst they are similar to fluids when the Deborah number is low. From this perspective, every material “flows” essentially, and bears elastic, viscous and plastic features simultaneously. However, under most external excitations only one or two characteristics are obviously visible and dominant, the rest, in comparison with the dominant features, can simply be neglected. The constitutive equation for the Cauchy stress tensor should thus be constructed to account for elastic, viscous and plastic features simultaneously in the very beginning, and can be further simplified for simpler situations when some characteristics are not significant.

Recently, based on the works of non-Newtonian fluids and rheology, an unified evolution equation for the Cauchy stress tensor of elasto-visco-plastic fluids is proposed in the

$$\mathbf{t} = -p\mathbf{I} + \mathbf{T}, \quad \mathbf{A}\mathbf{T} + \lambda_1 \left\{ (1 - \xi)\overset{\nabla}{\mathbf{T}} + \xi\overset{\Delta}{\mathbf{T}} \right\} = 2\mu \left(\mathbf{D} + \lambda_2 \overset{\nabla}{\mathbf{D}} \right) + \mathbf{N} + \varepsilon \mathbf{D}^n, \quad (1.1)$$

with the definitions $\overset{\nabla}{\mathbf{A}} = \dot{\mathbf{A}} - \mathbf{L}\mathbf{A} - \mathbf{A}\mathbf{L}^T$, $\overset{\Delta}{\mathbf{A}} = \dot{\mathbf{A}} + \mathbf{L}^T\mathbf{A} + \mathbf{A}\mathbf{L}$, known as the upper-convected and lower-convected time derivatives, respectively, for a tensor-valued variable \mathbf{A} . In Eqn. 1.1 the quantity p is the pressure, which is not defined conventionally, \mathbf{I} the second-rank identity tensor, \mathbf{T} the extra stress tensor, \mathbf{L} the velocity gradient, \mathbf{D} the symmetric part of \mathbf{L} and \mathbf{N} an unspecified non-linear, tensor-valued function. \mathbf{N} is ascribed the effects of plasticity, hypoplasticity and hypoelasticity [3]. The superscript T denotes transposition.

Λ , λ_1 , ξ , μ , λ_2 , ε and n are scalar coefficients; they are in general non-constant and may depend on the scalar invariants of the state of the material. In particular, λ_1 , μ , λ_2 and ε are recognized as relaxation time, viscosity, retardation time and a dissipative and turbulence parameter, respectively, provided that $\Lambda=1$. $\dot{\varphi}$ denotes the material time derivative of φ . By assigning different values to Λ , λ_1 , ξ , μ , λ_2 , ε , N and n , various models in the field of non-Newtonian fluids such as the Oldroyd-B model, the Maxwell-A and -B models, the Johnson-Segalman model, the Criminale-Erickson-Filbey model, the Reiner-Rivlin and the Bingham models can be reproduced [3].

Apparently, all the parameters in Eqn. 1.1 should be so constrained that the model is thermodynamically consistent, i.e., during a physical-realizable process the quantity, namely the entropy production, should be non-negative, while the balance and constitutive equations are satisfied simultaneously. Such an analysis has been performed and the results show that while the scalar parameters are related to the Helmholtz free energy and are determined once the free energy is prescribed, the unspecific tensor-valued function N plays an interesting role in the model: different plastic characteristics can enter the model via its prescription [3]. This result is in particular significant, since the thermodynamic foundation of hypoplasticity, a well-known class of constitutive relations for granular and porous materials, has been established rationally. The model was subsequently employed to study the normal stress effects in the context of a viscometric flow, and a time-dependent flow between two infinite parallel plates driven by a sudden motion of the plate, to estimate its performance and limitations [4]. Results show that the transient behavior of the fluid from its start-up to steady state can appropriately be indexed by varying the model parameters. In particular, different spectra of relaxation and retardation, the transmission of the shear and the emerging non-Newtonian characteristics can be accounted for by the model. These findings suggest a possible applicability of the present stress model in the fields of geomorphic fluid motions like soils movements and granular/debris flows.

In the present study, the stress model is applied to study the cyclic responses of a confined elasto-visco-plastic fluid driven by an externally oscillating excitation, to simulate the behavior of a granular material under cyclic loading, e.g. the transient responses of the soils between two parallel plates induced by an oscillating seismic activity. To this end, the governing equation, boundary conditions and the discussions on the numerical results of the considered problem are provided in Sect. 2. The paper is summarized in Sect. 3. For convenience, the balance equations of elasto-visco-plastic fluids in isothermal motions for mass, linear momentum and angular momentum are given respectively by

$$0 = \dot{\rho} + \rho \operatorname{div} \mathbf{v}, \quad \mathbf{0} = \rho \dot{\mathbf{v}} - \operatorname{div} \mathbf{t} - \rho \mathbf{b}, \quad \mathbf{0} = \mathbf{t} - \mathbf{t}^T, \quad (1.2)$$

where ρ is the density, \mathbf{v} the velocity and \mathbf{b} the specific body force. In the formulations the fluid is not considered micropolar or Cosserat-type, so that the balance of angular momentum reduces to its simplest form, namely the symmetry of the Cauchy stress tensor, which is fulfilled automatically by the stress model Eqn. 1.1, provided that N is symmetric. In addition, for isothermal flows the balance of internal energy is not relevant and is omitted for simplicity.

2. UNSTEADY FLOW BETWEEN TWO PARALLEL PLATES

Consider an incompressible, isothermal elasto-visco-plastic fluid between two parallel plates with the prescribed configuration and the coordinate system shown in Figure 1. Initially, both the fluid and the two plates are stationary. At a prescribed time, the lower plate starts to oscillate with a specific frequency ω and amplitude V_0 , which triggers the motion of the fluid through the shear stress between the lower plate and the fluid immediately above it.

Since the flow is triggered by the relative motion between the fluid and the plate, it is plausible to assume that parallel flow prevails, namely,

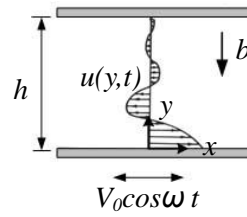


Figure 1. Sketch of an unsteady flow between two parallel plates driven by the oscillating motion of the lower plate and the coordinate system

$$\mathbf{v} = [u(y), 0, 0], \quad p = p(y), \quad \mathbf{b} = [0, -b, 0], \quad (2.1)$$

hold, where $u(y)$ is the velocity component in the x -direction. From this perspective, it is reasonable to assume that the extra stress tensor \mathbf{T} takes the form

$$\mathbf{T} = \begin{pmatrix} T_{xx}(y) & T_{xy}(y) & 0 \\ T_{yx}(y) & T_{yy}(y) & 0 \\ 0 & 0 & 0 \end{pmatrix}. \quad (2.2)$$

Substituting Eqns. 2.1 and 2.2 into Eqn. 1.2₂ gives rise to the balance of linear momentum in the reduced forms

$$\frac{\partial u}{\partial t} = \frac{\partial T_{xy}}{\partial y}, \quad 0 = -\frac{\partial p}{\partial y} + \frac{\partial T_{yy}}{\partial y} - \rho b, \quad (2.3)$$

which are the balances of linear momentum in the x - and y -directions, respectively. Eqn. 2.3₂ indicates that the combination of $-p + T_{yy}$ constructs a “hydrostatic” linear profile; the pressure p is thus determined once T_{yy} and its boundary values are prescribed. Eqn. 2.3₁ emerges as a time-dependent PDE for the velocity profile $u(y, t)$, provided that T_{xy} can be expressed as a function of $u(y, t)$. We should discuss it later on. Moreover, it is noted that with the parallel flow assumption the balance of mass Eqn. 1.2₁ is automatically fulfilled.

To obtain an implicit expression of the extra stress tensor component T_{xy} from (1), the tensor-valued function N needs be prescribed. It has been demonstrated that the effects of plastic deformation and the transient behavior of materials can better be indexed when a hypoplastic expression is assigned to N [4]. In the present study we follow the same approach, and N is thus given by [5,6]

$$\mathbf{N} = \left(C_1 \mathbf{T} + C_2 \frac{\mathbf{T}\mathbf{T}}{\text{tr}\mathbf{T}} \right) \|\mathbf{D}\|, \quad \|\mathbf{D}\| = \sqrt{\text{tr}\mathbf{D}^2} \quad (2.4)$$

where $C_{1,2}$ are again model parameters, which can depend on the state of the motion. Eqn. 2.4 is the common hypoplastic expression [6,7,8], which is essentially a non-linear incremental expression for the stress-stretching relation with two distinct features: (i) distinction between loading and unloading of the material is automatically accomplished; and (ii) elastic/inelastic deformations need not *a priori* be distinguished, and hence information about yield surface and plastic potential is no longer necessary. In view of the parallel flow assumption Eqn. 2.1₁ and the extra stress tensor components Eqn. 2.2, the components of N take the forms

$$\mathbf{N} = \begin{pmatrix} N_{xx}(y) & N_{xy}(y) & 0 \\ N_{yx}(y) & N_{yy}(y) & 0 \\ 0 & 0 & 0 \end{pmatrix}, \quad (2.5)$$

in which $N_{xy} = N_{yx}$ to fulfill the symmetry of the Cauchy stress tensor.

Identifying the components of \mathbf{N} by using Eqn. 2.4 and substituting the results into Eqn. 1.1 with the definition Eqn. 2.2 yields the constitutive expressions of the components of the extra stress tensor in the implicit forms

$$\begin{aligned} \Delta T_{xx} + \lambda_1 \left[\frac{\partial T_{xx}}{\partial t} - 2(1-\xi)T_{xy} \frac{\partial u}{\partial y} \right] &= -2\mu\lambda_2 \left(\frac{\partial u}{\partial y} \right)^2 + \frac{\sqrt{2}}{2} \left| \frac{\partial u}{\partial y} \right| \left(C_1 T_{xx} + \frac{C_2}{tr\mathbf{T}} (T_{xx}^2 + T_{yy}^2) \right), \\ \Delta T_{xy} + \lambda_1 \left[\frac{\partial T_{xy}}{\partial t} - (1-\xi)T_{yy} \frac{\partial u}{\partial y} + \xi T_{xx} \frac{\partial u}{\partial y} \right] &= \mu \frac{\partial u}{\partial y} + \mu\lambda_2 \frac{\partial^2 u}{\partial t \partial y} + \frac{\sqrt{2}}{2} \left| \frac{\partial u}{\partial y} \right| \left(C_1 T_{xy} + \frac{C_2}{tr\mathbf{T}} (T_{xx}T_{xy} + T_{xy}T_{yy}) \right), \\ \Delta T_{yy} + \lambda_1 \left[\frac{\partial T_{yy}}{\partial t} + 2\xi T_{xy} \frac{\partial u}{\partial y} \right] &= \frac{\sqrt{2}}{2} \left| \frac{\partial u}{\partial y} \right| \left(C_1 T_{yy} + \frac{C_2}{tr\mathbf{T}} (T_{xy}^2 + T_{yy}^2) \right). \end{aligned} \quad (2.6)$$

The governing equation for the velocity distribution $u(y,t)$ can be obtained in principle by substituting the constitutive relations Eqn. 2.6 into the balance equation Eqn. 2.3₁, resulting in a time-dependent, nonlinear second-order partial differential equation, subjected to the traditional non-slip boundary conditions on the upper and lower plates given by

$$u(y=0,t) = V_0 \cos \omega t, \quad u(y=h,t) = 0, \quad (2.7)$$

respectively. The emerging two-point initial and boundary value problem should be solved numerically for variations of the model parameters. However, for numerical simplicity we let the balance and constitutive equations be expressed separately.

Nondimensionalization. Defining the dimensionless parameters according to

$$\begin{aligned} \bar{y} &= \frac{\omega y}{V}, \quad \bar{u} = \frac{u}{V_0}, \quad \bar{t} = \omega t, \quad \bar{\mathbf{T}} = \frac{\mathbf{T}}{\rho V_0^2}, \quad \beta_1 = \frac{\omega \lambda_1}{\Lambda}, \\ \beta_2 &= \frac{\omega \mu}{\rho V_0^2 \Lambda}, \quad \beta_3 = \frac{\omega \lambda_2}{\Lambda}, \quad \beta_4 = \frac{\omega C_{10}}{\Lambda}, \quad \beta_5 = \frac{\omega C_2}{\Lambda}, \end{aligned} \quad (2.8)$$

and substituting Eqn. 2.8 into Eqns. 2.3₁, 2.6 and 2.7 gives rise to the dimensionless balance equation and the associated boundary conditions in the forms

$$\frac{\partial \bar{u}}{\partial \bar{t}} = \frac{\partial \bar{T}_{xy}}{\partial \bar{y}}, \quad \bar{u}(0, \bar{t}) = \cos \bar{t}, \quad \bar{u}(\bar{y} = \bar{h}, \bar{t}) = 0, \quad (2.9)$$

where $\bar{h} = \omega h / V_0$, and the components of the dimensionless extra stress tensor are given by

$$\begin{aligned} \bar{T}_{xx} + \beta_1 \left[\frac{\partial \bar{T}_{xx}}{\partial \bar{t}} - 2(1-\xi)\bar{T}_{xy} \frac{\partial \bar{u}}{\partial \bar{y}} \right] &= -2\beta_2\beta_3 \left(\frac{\partial \bar{u}}{\partial \bar{y}} \right)^2 + \frac{\sqrt{2}}{2} \left| \frac{\partial \bar{u}}{\partial \bar{y}} \right| \left(\beta_4 \bar{T}_{xx} + \frac{\beta_5}{tr\bar{\mathbf{T}}} (\bar{T}_{xx}^2 + \bar{T}_{yy}^2) \right), \\ \bar{T}_{xy} + \beta_1 \left[\frac{\partial \bar{T}_{xy}}{\partial \bar{t}} - (1-\xi)\bar{T}_{yy} \frac{\partial \bar{u}}{\partial \bar{y}} + \xi \bar{T}_{xx} \frac{\partial \bar{u}}{\partial \bar{y}} \right] &= \beta_2 \frac{\partial \bar{u}}{\partial \bar{y}} + \beta_2\beta_3 \frac{\partial^2 \bar{u}}{\partial \bar{t} \partial \bar{y}} + \frac{\sqrt{2}}{2} \left| \frac{\partial \bar{u}}{\partial \bar{y}} \right| \left(\beta_4 \bar{T}_{xy} + \frac{\beta_5}{tr\bar{\mathbf{T}}} (\bar{T}_{xx}\bar{T}_{xy} + \bar{T}_{xy}\bar{T}_{yy}) \right), \\ \bar{T}_{yy} + \beta_1 \left[\frac{\partial \bar{T}_{yy}}{\partial \bar{t}} + 2\xi \bar{T}_{xy} \frac{\partial \bar{u}}{\partial \bar{y}} \right] &= \frac{\sqrt{2}}{2} \left| \frac{\partial \bar{u}}{\partial \bar{y}} \right| \left(\beta_4 \bar{T}_{yy} + \frac{\beta_5}{tr\bar{\mathbf{T}}} (\bar{T}_{xy}^2 + \bar{T}_{yy}^2) \right). \end{aligned} \quad (2.10)$$

While the dimensionless parameters β_1 and β_3 are respectively used to account for the effects of relaxation and retardation (effects of elasticity), the parameter β_2 is for the viscous effect and β_4 and β_5 are for the hypoplastic effects. Eqns. 2.9 and 2.10 define the dimensionless governing equation and the boundary conditions for the considered problem, and should be solved to obtain the profiles of $\bar{u}(\bar{y}, \bar{t})$ for variations of the parameters β_{1-5} . However, increasing the value of β_3 counteracts the effects caused by increasing β_1 for the considered problem. To reduce such an influence, β_3 is kept to be a constant, namely 1.0, in all the calculations. In addition, variation of ξ affects only the weights of the upper- and lower-convective derivatives of \mathbf{T} and has no significant influence on the results. It is chosen to be 0.5 through the calculations. Moreover, \bar{h} indicates the influences of the upper stationary solid boundary; it should be so chosen that the influences of the boundary layer can be taken into account. For convenience, it is chosen to be 0.5 in the numerical simulations (this will be discussed later).

Numerical method. The emerging two-point IBV problem Eqns. 2.9 and 2.10 are solved numerically by using finite difference method. In particular, we discretize the space domain by using the central-difference scheme, while the time domains for \bar{u} and $\bar{\mathbf{T}}$ are discretized by using the first-order backward and forward difference approximations, respectively. The solutions of $\bar{u}(\bar{y}, \bar{t})$ are obtained by using explicit method [9]: for better numerical convergence and stability $\Delta \bar{t} < 10^{-6}$ should be fulfilled in associated with the $\Delta \bar{y}$ -domain discretized into 10^3 equal-spacings in most cases.

Numerical results. Typical calculated results for the velocity distribution $\bar{u}(\bar{y}, \bar{t})$ are shown in Figures 2-5, in which the solid curves are the results from the present model, while the dotted curves are calculated from the formula

$$\bar{u} = Re \left[\left(\frac{e^{(1+i)\alpha\bar{y}}}{1 - e^{(1+i)\alpha\bar{h}}} - \frac{e^{(1+i)\alpha(2\bar{h}-\bar{y})}}{1 - e^{(1+i)2\alpha\bar{h}}} \right) e^{i2\pi\bar{t}} \right], \quad (2.11)$$

where $\alpha = \sqrt{\pi/\beta_2}$. Eqn. 2.11 is the analytical solution of Newtonian fluid in complex form and can be derived from [10]. Figure 2(a) illustrates the typical profiles of $\bar{u}(\bar{y}, \bar{t})$ for the time domain $\bar{t} = 0$ to $\bar{t} = \pi$ increased by $\pi/6$ for clarity, in which the orders of magnitude of the parameters are the same and are given by $\beta_1 = \beta_2 = \beta_4 = \beta_5 = 0.1$. It is seen that due to the combined elastic, viscous and plastic effects, the shear generated on the oscillating plate can better be transmitted toward the stationary plate in the present model. The phase lag is relatively insignificant in comparison with the results from Newtonian fluid. To show the influences of the upper stationary boundary, calculations have also been made for variations of \bar{h} ; the results are displayed in Figure 2(b), in which the profiles of $\bar{u}(\bar{y}, \bar{t})$ at $\bar{t} = \pi/2$ for $\bar{h} = 0.5, 1.0$, and ∞ are plotted. When \bar{h} is greater than the boundary layer thickness, the upper solid boundary has no influence on the velocity profile. On the contrary, when \bar{h} is smaller than the boundary layer thickness, the upper solid boundary will enhance the decay of the flow, and such an influence is more visible in the Newtonian model than in the present model. This implies that the transmission of the shear is more efficient in the present model when the combined elastic, viscous and plastic characteristics of the material are account for. Similarly, the phase lag in the present model is relatively insignificant in comparison with the Newtonian fluid, regardless the value of \bar{h} .

Figure 3(a) illustrates the calculated profiles of $\bar{u}(\bar{y}, \bar{t})$ at different time slices for the limiting case in which the elastic effect is dominant, and the values of the parameters are given by $\beta_1 = 0.5$ and $\beta_2 = \beta_4 = \beta_5 = 0.1$. In such a situation the relaxation time increases, and the fluid needs a longer time to adjust itself to the variation of the external excitation, which is relevant in the more convex velocity profiles above the oscillating boundary when compared with Figure 2(a). Increasing the value of β_1 tends to enhance the elastic effects of the fluid, as shown in Figure 3(b), in which a time series of the velocity profiles at the middle of the channel for various values of

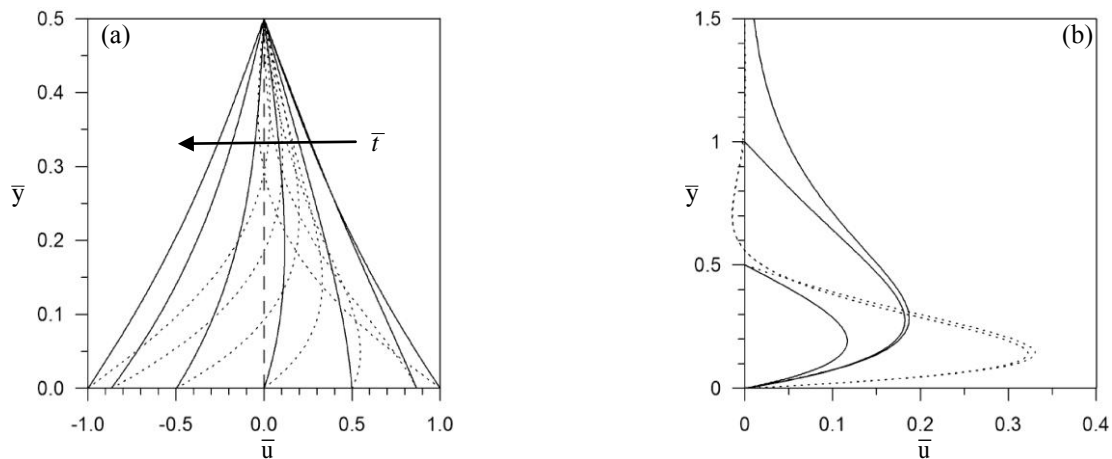


Figure 2. (a) Calculated velocity profiles at different time slices $\bar{t} = [0, \pi/6, \pi/3, \pi/2, 2\pi/3, 5\pi/6, \pi]$, (b) velocity profiles at $\bar{t} = \pi/2$ for different values of $\bar{h} = 0.5, 1.0$ and ∞ . In (a)-(b): $\beta_1 = \beta_2 = \beta_4 = \beta_5 = 0.1$, solid: present model; dotted: Newtonian fluid

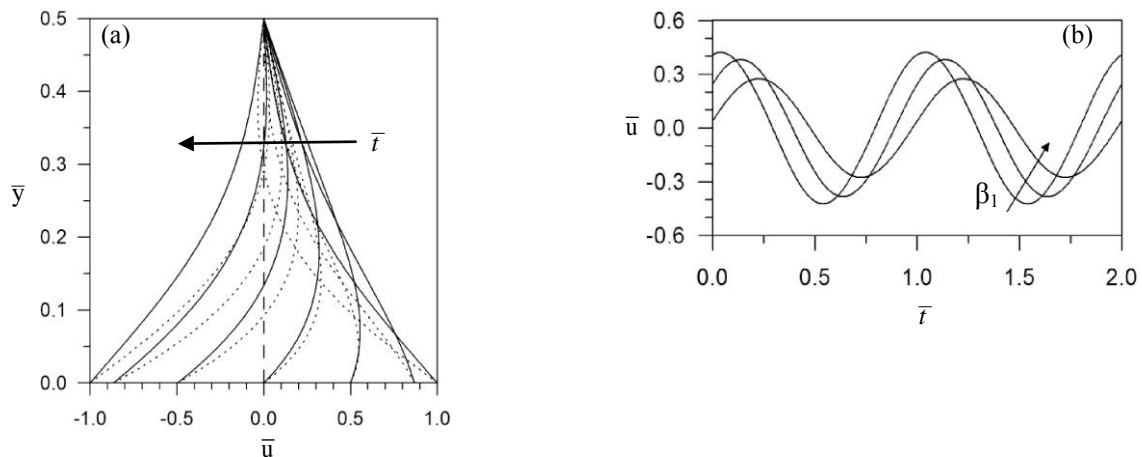


Figure 3. (a) Calculated velocity profiles at different time slices $\bar{t} = [0, \pi/6, \pi/3, \pi/2, 2\pi/3, 5\pi/6, \pi]$ and $\beta_1 = 0.5$, (b) time series of the velocity profiles at $\bar{y} = 0.25$ (the middle of the channel) and $\beta_1 = 0.1, 0.5, 1.0$. In (a)-(b): $\beta_2 = \beta_4 = \beta_5 = 0.1$, solid: present model; dotted: Newtonian fluid

β_1 versus \bar{t} is plotted. When the value of β_1 is small, the phase lag is mainly due to the combined elastic, viscous and hypoplastic effects, and is relatively insignificant, while the amplitude preserves a certain amount of its boundary value V_0 . On the contrary, when β_1 is large, the elastic effect increases: the most part of the energy supplied by the oscillating boundary is preserved in the fluids immediately above the solid boundary, resulting in a smaller velocity amplitude at the middle of the channel. The phase lag, as a result, becomes larger at the middle of the channel.

Figure 4(a) shows the calculated results of the velocity profiles when the viscous effect is dominant: the values of the parameters are given by $\beta_2 = 0.5$ and $\beta_1 = \beta_4 = \beta_5 = 0.1$. It is seen that the obtained velocity profiles are fairly straight across the channel, for the shear is more efficiently transmitted by the larger viscous effects. Such a tendency is also manifest in Figure 4(b), in which again a time series of the velocity profiles at the middle of the channel is plotted for variations of β_2 . When β_2 is small, the viscous effect is not significant and the energy supplied by the oscillating boundary is mainly preserved in the fluids immediately above the oscillating boundary by the combined elastic and hypoplastic effects, resulting in a smaller amplitude and larger phase lag of the velocity profile at the middle of the channel. However, when the value of β_2 is high, the adhesion between different layers of the fluids and the boundary enhances correspondingly, such that the fluid can adjust

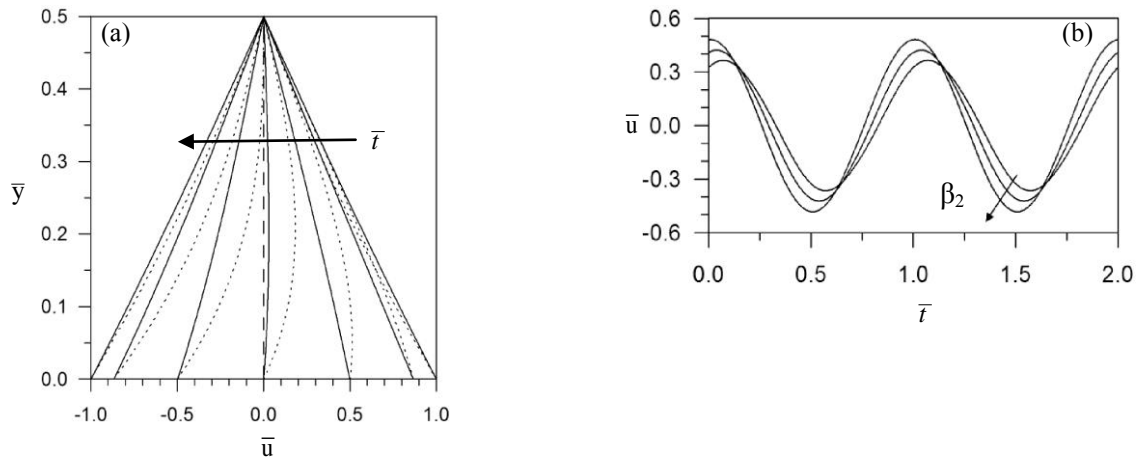


Figure 4. (a) Calculated velocity profiles at different time slices $\bar{t} = [0, \pi/6, \pi/3, \pi/2, 2\pi/3, 5\pi/6, \pi]$ and $\beta_2=0.25$, (b) time series of the velocity profiles at $\bar{y} = 0.25$ (the middle of the channel) and $\beta_2=0.05, 0.1, 0.5$. In (a)-(b): $\beta_1=\beta_4=\beta_5=0.1$, solid: present model; dotted: Newtonian fluid

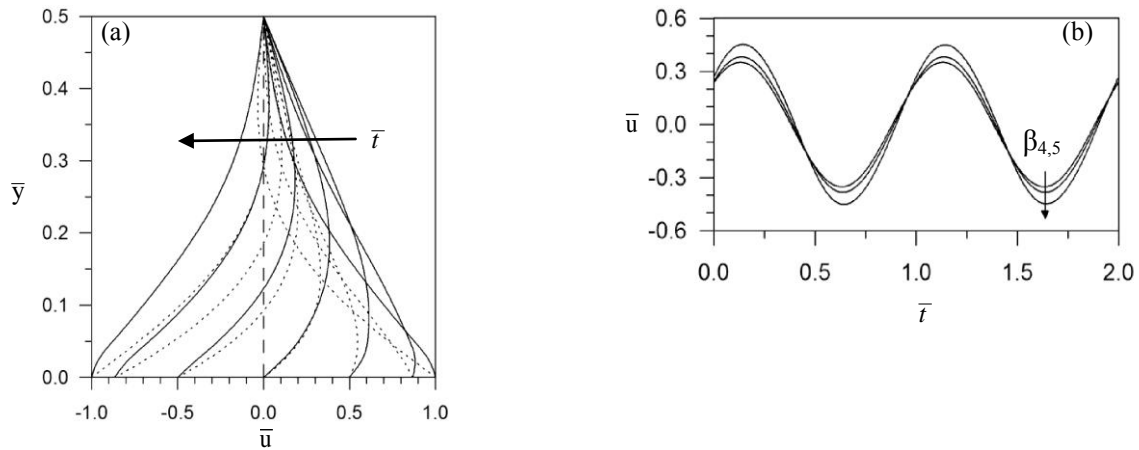


Figure 5. (a) Calculated velocity profiles at different time slices $\bar{t} = [0, \pi/6, \pi/3, \pi/2, 2\pi/3, 5\pi/6, \pi]$ and $\beta_4=\beta_5=0.25$, (b) time series of the velocity profiles at $\bar{y} = 0.25$ (the middle of the channel) and $\beta_4=\beta_5= 0, 0.1, 0.25$. In (a)-(b): $\beta_1=\beta_2= 0.1$, solid: present model; dotted: Newtonian fluid

itself to the variation of the external excitation in a faster way, resulting in larger amplitude and smaller phase lag of the velocity profiles at the middle of the channel.

Calculations for the velocity profiles in which the hypoplastic effect is dominant have also been performed and are shown in Figure 5(a), in which the parameters are given by $\beta_1=\beta_2=0.1$ and $\beta_4=\beta_5=0.25$. When hypoplastic effect is significant, plastic deformation occurs in the region immediately above the solid boundary. At the time slices at which the oscillating boundary changes its state of motion (e.g. at $\bar{t} = 0$ and $\bar{t} = \pi$, the oscillating plate changes its motion direction), the fluid immediately above the boundary moves with the same direction of the boundary due to the viscous effect. However, fluids above this layer hold the previous motion direction due to the plastic deformation. These give rise to the more convex velocity profiles near the oscillating boundary, when compared with Figure 3(a). Such a tendency is also relevant in the time series of the velocity profiles at the middle of the channel for variations of the values of β_4 and β_5 , as shown in Figure 5(b). When β_4 and β_5 increase, plastic deformation above the oscillating boundary becomes stronger (and hence the velocity profiles there become sharper), resulting in larger amplitude of the velocity profiles at the center of the channel. However, due to the plastic deformation the phase lag only increases slightly, when compared with Figure 3(b).

3. CONCLUDING REMARKS

The main conclusions are summarized in the following:

- For unsteady parallel flows the shear generated on the oscillating boundary can better be transmitted toward the fluids when the elastic, viscous and plastic features of the fluids are taken into account for simultaneously. The penetration of the influence of the moving boundary is enhanced significantly in the present model than in the Newtonian model. Such an influence can be recognized by higher values of the boundary layer thickness.
- When elastic effect increases, the fluid needs a longer time to adjust itself to the variation of the oscillating boundary. The most part of the shear energy is preserved in the region near the moving boundary. These give rise to the convex velocity profiles near the oscillating plate, and the velocity profiles with smaller amplitude and larger phase lag in the upper part of the flow field.
- As viscosity increases, the adhesion between different layers of fluids and the solid boundary increases correspondingly. As a result, the shear can be transmitted most efficiently, and fairly "straight" velocity profiles across the flow field are obtained. Since the viscous effect is dominant, the fluid can response to the variation of the external excitation (here the oscillating plate) in a faster way, resulting smaller phase lag of the velocity profiles.
- By higher hypoplastic effect, plastic deformation occurring near the oscillating boundary is enhanced. This yields more convex velocity profiles near the oscillating plate in comparison with those from the cases of higher elastic effects, and are in particular visible when the oscillating boundary suddenly changes its motion direction. The amplitude of the velocity profiles in the upper part of the flow field increases as the hypoplastic effect increases; however, the phase lag only increases slightly due to the enhanced plastic deformation near the oscillating plate.

ACKNOWLEDGEMENTS

The authors are indebted to the Taiwan Science Council for the financial support through the funding grant NSC 96-2221-E-006-078-MY3.

REFERENCES

- [1] Tanner, R.I. (1992). Engineering Rheology, Oxford University Press, Oxford New York Toronto
- [2] Truesdell, C. and Noll, W. (1965). The Non-linear Theories of Mechanics, In: Handbuch der Physik, III/3, (Flügge S. ed.), Springer Verlag, Berlin Heidelberg New York
- [3] Fang, C., Wang, Y. and Hutter, K. (2008). A unified evolution equation for the Cauchy stress tensor of an isotropic elasto-visco-plastic material. I. On thermodynamically consistent evolution. *Continuum Mech. Thermodyn.* **19:7**, 432--440
- [4] Fang, C., Lee, C.H. (2008). A unified evolution equation for the Cauchy stress tensor of an isotropic elasto-visco-plastic material. II. Normal stress difference in a viscometric flow, and an unsteady flow with a moving boundary. *Continuum Mech. Thermodyn.* **19:7**, 441--455
- [5] Kolymbas, D. (1991). An outline of hypoplasticity. *Arch. Appl. Mech.* **61**, 143--151
- [6] Kolymbas, D. (2000). Introduction to Hypoplasticity, Balkema, Rotterdam
- [7] Wu, W. (2006). On high-order hypoplastic models for granular materials, *J. Eng. Math.* **56**, 23--34
- [8] Wu, W. and Kolymbas, D. (2000). Hypoplasticity then and now. In: Constitutive Modelling of Granular Materials, (Kolymbas, D. ed.), Springer Verlag, Berlin Heidelberg New York, 57--105
- [9] Anderson, D.A., Tannehill, J.C. and Pletcher, R.H. (1984). Computational Fluid Mechanics and Heat Transfer, McGraw-Hill, New York
- [10] White, F.M. (1991). Viscous Fluid Flow, 2nd ed., McGraw-Hill Book Co., New York

The 14th World Conference on Earthquake Engineering
October 12-17, 2008, Beijing, China

